CELL DEATH

Copper induces cell death by targeting lipoylated TCA cycle proteins

Peter Tsvetkov[1]*, Shannon Coy[2,3,4,5], Boryana Petrova[5,6], Margaret Dreishpoon[1], Ana Verma[2,3,4,5], Mai Abdusamad[1], Jordan Rossen[1], Lena Joesch-Cohen[1], Ranad Humeidi[1], Ryan D. Spangler[1], John K. Eaton[1], Evgeni Frenkel[7], Mustafa Kocak[1], Steven M. Corsello[1,5,8], Svetlana Lutsenko[9], Naama Kanarek[1,5,6], Sandro Santagata[2,3,4,5,10], Todd R. Golub[1,5,11,12]*

Copper is an essential cofactor for all organisms, and yet it becomes toxic if concentrations exceed a threshold maintained by evolutionarily conserved homeostatic mechanisms. How excess copper induces cell death, however, is unknown. Here, we show in human cells that copper-dependent, regulated cell death is distinct from known death mechanisms and is dependent on mitochondrial respiration. We show that copper-dependent death occurs by means of direct binding of copper to lipoylated components of the tricarboxylic acid (TCA) cycle. This results in lipoylated protein aggregation and subsequent iron-sulfur cluster protein loss, which leads to proteotoxic stress and ultimately cell death. These findings may explain the need for ancient copper homeostatic mechanisms.

The requirement of copper as a cofactor for essential enzymes has been recognized across the animal kingdom, spanning bacteria to human cells (*1*). However, intracellular copper concentrations are kept at extraordinarily low levels by active homeostatic mechanisms that work across concentration gradients to prevent the accumulation of free intracellular copper that is detrimental to cells (*1*–*4*). Whereas the mechanisms of toxicity of other essential metals, such as iron, are well established, the mechanisms of copper-induced cytotoxicity remain unclear (*5*–*7*).

Copper ionophores are copper-binding small molecules that shuttle copper into the cell and are thereby useful tools to study copper toxicity (*8*, *9*). Multiple lines of evidence indicate that the mechanism of copper ionophore–induced cell death involves intracellular copper accumulation and not the effect of the small molecule chaperones themselves. Multiple, structurally distinct small molecules that bind copper share killing profiles across hundreds of cell lines [Fig. 1A, fig. S1A, and (*5*, *10*)]. Structure-function relationship experiments show that modifications that abrogate the copper binding capacity of these compounds result in loss of cell killing (*5*), and copper chelation eliminates the cytotoxicity of the compounds [fig. S1, B to C, and (*5*)].

A clear picture of the mechanisms underlying copper-induced toxicity has not yet emerged, with contradictory reports suggesting either the induction of apoptosis (*11*, *12*), caspase-independent cell death (*5*, *7*, *13*), reactive oxygen species (ROS) induction (*14*–*16*), or inhibition of the ubiquitin-proteasome system (*17*–*19*). The cross-kingdom efficacy of copper-binding molecules as cell death inducers suggests that they target evolutionarily conserved cellular machinery, but such mechanisms have yet to be elucidated.

To further establish whether copper ionophore cytotoxicity is dependent on copper itself, we analyzed the killing potential of the potent copper ionophore elesclomol. The source of copper in cell culture medium is serum (fig. S1D), and accordingly, cells grown in the absence of serum were resistant to elesclomol. By contrast, elesclomol sensitivity was completely restored by the addition of copper in a 1:1 ratio (fig. S1, E and F). Copper supplementation similarly sensitized cells to treatment with six structurally distinct copper ionophores (Fig. 1B and fig. S1, G to P), but supplementation with other metals, including iron, cobalt, zinc, and nickel, failed to potentiate cell death (Fig. 1B and fig. S1, G to P). Consistent with this observation, depletion of the endogenous intracellular copper chelator glutathione, using buthionine sulfoximine (BSO), sensitized cells to elesclomol-copper–induced cell death (fig. S1Q), whereas chelation of copper with tetrathiomolybdate (TTM) rescued killing (fig. S1, B and C) and chelators of other metals had no effect (fig. S1R). Lastly, a 2-hour pulse treatment with potent copper ionophores (elesclomol, disulfiram, and NSC319726) resulted in a ~5- to 10-fold increase in levels of intracellular copper but not zinc (fig. S2A). These results suggest that copper ionophore–induced cell death is primarily dependent on intracellular copper accumulation.

Copper ionophores induce a distinct form of regulated cell death

We first asked whether copper ionophore–mediated cell death is regulated and specifically whether short-term exposure leads to irrevocable, subsequent cell cytotoxicity. Pulse treatment with the copper ionophore elesclomol at concentrations as low as 40 nM for only 2 hours resulted in a 15- to 60-fold increase in intracellular copper levels (fig. S2, B and C) that triggered cell death more than 24 hours later (Fig. 1C). This result suggests that copper-mediated cell death is indeed regulated.

Cell death involves signaling cascades and molecularly defined effector mechanisms (*20*) that involve proteins and lipids such as those characteristic of apoptosis (*21*), necroptosis (*22*), pyroptosis (*23*), and ferroptosis (*24*), which is a recently discovered iron-dependent cell death pathway. Previous reports suggested that elesclomol induces ROS-dependent apoptotic cell death (*6*, *12*), but elesclomol-induced cell death did not involve either the cleavage or activation of caspase 3 activity, the hallmark of apoptosis (*25*) (Fig. 1, D and E, and fig. S2D). Similarly, elesclomol killing potential was maintained when the key effectors of apoptosis, BAX and BAK1, were knocked out (Fig. 1F and fig. S2, E to I) or when cells were cotreated with pan-caspase inhibitors (Z-VAD-FMK and Boc-D-FMK) (Fig. 1G), again indicating that the copper-induced cell death is distinct from apoptosis. Furthermore, treatment with inhibitors of other known cell death mechanisms—including ferroptosis (ferrostatin-1), necroptosis (necrostatin-1), and oxidative stress (*N*-acetyl cysteine)—all failed to abrogate copper ionophore–induced cell death (Fig. 1G), suggesting a mechanism distinct from known cell death pathways (Fig. 1H).

Mitochondrial respiration regulates copper ionophore–induced cell death

One hint to the pathways that mediate copper ionophore–induced cell death is the observation that cells that are more reliant on mitochondrial respiration are nearly 1000-fold more sensitive to copper ionophores than cells undergoing glycolysis (Fig. 2A and fig. S3, A to F). Treatment with mitochondrial antioxidants, fatty acids, and inhibitors of mitochondrial function had a very distinct effect on the sensitivity to copper ionophores as compared with sensitivity to the ferroptosis-inducing GPX4 inhibitor ML162 (Fig. 2B). Furthermore, inhibitors of complexes I and II of the electron transport chain (ETC) as well as inhibitors of mitochondrial pyruvate uptake attenuated cell death with no effect on ferroptosis (Fig. 2B). Importantly, the mitochondrial uncoupler FCCP had no effect on copper toxicity, suggesting that mitochondrial respiration, not

[1]Broad Institute of Harvard and MIT, Cambridge, MA, USA. [2]Laboratory of Systems Pharmacology, Department of Systems Biology, Boston, MA, USA. [3]Ludwig Center at Harvard, Harvard Medical School, Boston, MA, USA. [4]Department of Pathology, Brigham and Women's Hospital, Boston, MA, USA. [5]Harvard Medical School, Boston, MA, USA. [6]Department of Pathology, Boston Children's Hospital, Boston, MA USA. [7]Whitehead Institute and Massachusetts Institute of Technology, Cambridge, MA, USA. [8]Department of Medical Oncology, Dana Farber Cancer Institute, Boston, MA, USA. [9]Department of Physiology, Johns Hopkins Medical Institutes, Baltimore, MD, USA. [10]Department of Pathology, Dana Farber Cancer Institute, Boston, MA, USA. [11]Department of Pediatric Oncology, Dana Farber Cancer Institute, Boston, MA, USA. [12]Division of Pediatric Hematology/Oncology, Boston Children's Hospital, Boston, MA, USA.
*Corresponding author. Email: ptsvetko@broadinstitute.org (P.T.); golub@broadinstitute.org (T.R.G.)

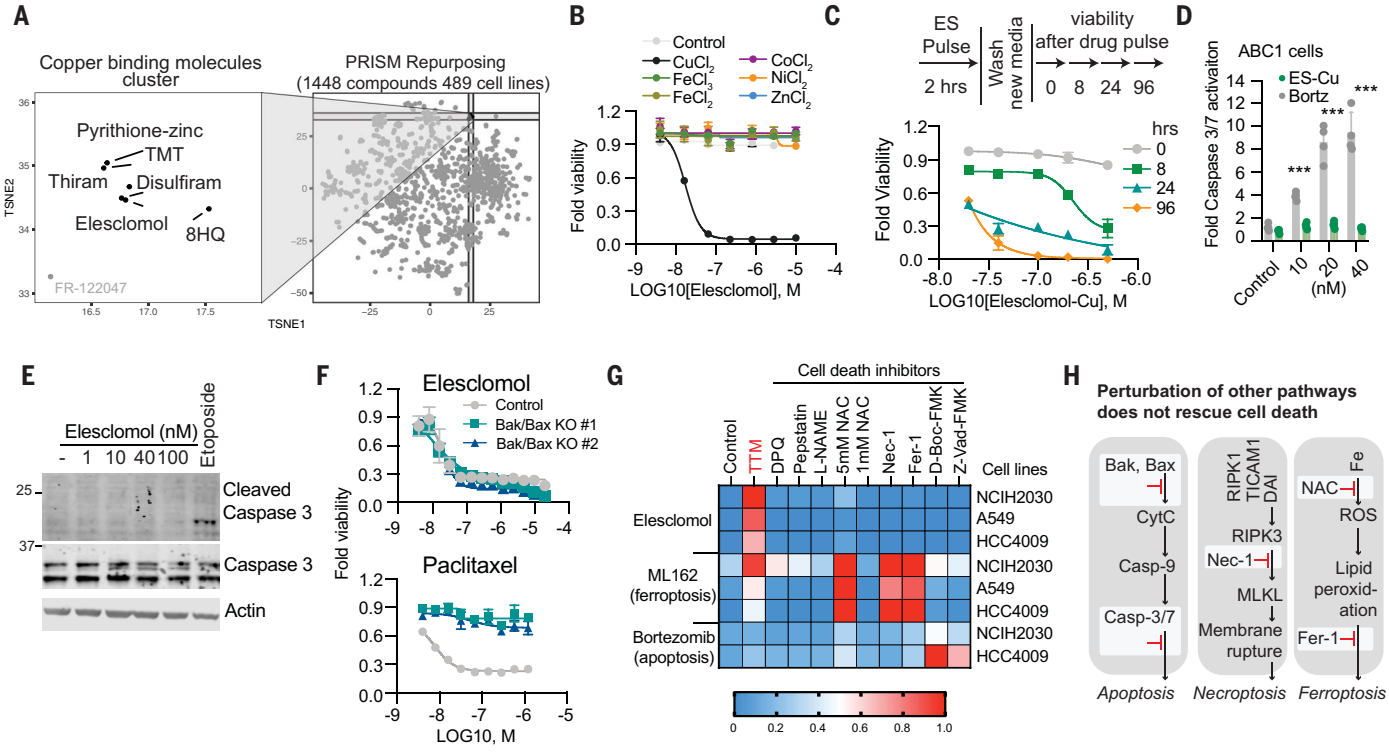

Fig. 1. Copper ionophore–induced cell death is nonapoptotic, nonferroptotic, and non-necroptotic. (**A**) PRISM (profiling relative inhibition simultaneously in mixtures) Repurposing secondary screen: Growth-inhibition estimates for 1448 drugs against 489 cell lines. TMT, tetramethylthiuram monosulfide; TSNE, t-distributed stochastic neighbor embedding. (**B**) Viability of cells (MON) after treatment with elesclomol with or without 10 μM of indicated metals. (**C**) Viability of ABC1 cells was assessed at the indicated times after elesclomol-Cu (1:1 ratio) pulse treatment and growth in fresh media. ES, elesclomol. (**D**) Caspase 3/7 cleavage in ABC1 cells 16 hours after indicted treatments (fold change over control). (**E**) Western blot analysis of G402 cells treated with the indicated concentrations of elesclomol or 25 μM etoposide for 6 hours. (**F**) Viability of HMC18 cells or two HMC18 clones with Bax/Bak deleted after treatment with elesclomol-$CuCl_2$ (1:1) (top) and paclitaxel (bottom). (**G**) Heatmap of viability of cells pretreated overnight with 20 μM necrostatin-1, 10 μM ferrostatin-1, 1 mM *N*-acetylcysteine (NAC), 5 mM *N*-acetylcysteine, 30 μM Z-VAD-FMK, 50 μM D-Boc-FMK, 20 μM TTM, 300 μM L-NAME, 1 μM pepstatin A, or 10 μM DPQ and then treated with either 30 nM elesclomol-$CuCl_2$ (1:1), 1 μM ML162 (GPX4 inhibitor), or 40 nM bortezomib for 72 hours (average of three replicates). (**H**) Schematic diagram of apoptosis, necroptosis, and ferroptosis. Inhibited pathways are marked in red. For (B), (D), and (F), data are means ± SD, with $n \geq 3$. For (D) and (E), media were supplemented with 1 μM $CuCl_2$.

adenosine triphosphate (ATP) production, is required for copper-induced cell death (Fig. 2C). Consistent with this finding, growing cells in hypoxic conditions (1% O_2) attenuated copper ionophore–induced cell death, whereas forced stabilization of the hypoxia-inducible factor (HIF) pathway with the HIF prolyl hydroxylase inhibitor FG-4592 under normoxic conditions (21% O_2) did not (Fig. 2D and fig. S3, G to J), further emphasizing the role of cellular respiration in mediating copper-induced cell death. However, treatment with copper ionophores did not induce significant reduction in basal or ATP-linked respiration but did significantly reduce the spare capacity of respiration (Fig. 2E and fig. S3, K to N), suggesting that copper does not target the ETC directly but rather components of the TCA cycle. In support of this, metabolite profiling of cells pulse-treated with elesclomol showed a time-dependent increase in metabolite dysregulation of many TCA cycle–associated metabolites in elesclomol-sensitive ABC1 cells but not in elesclomol-resistant A549 cells (fig. S3, O to S, and table S1). These results establish a link between copper ionophore–induced cell death and mitochondrial metabolism, not the ETC (Fig. 2F), leading us to further elucidate the precise connection between copper and the TCA cycle.

FDX1 and protein lipoylation are the key regulators of copper ionophore–induced cell death

To identify the specific metabolic pathways that mediate copper toxicity, we performed genome-wide CRISPR-Cas9 loss-of-function screens to identify the genes involved in copper ionophore–induced death. To maximize the generalizability of the screen, we focused on the intersection of two structurally distinct copper-loaded ionophores (elesclomol and the active form of disulfiram, diethyldithiocarbamate) (Fig. 3, A to C, and table S2). Killing by both compounds was rescued by knockout of seven genes (Fig. 3A, marked in blue), including *FDX1* [which encodes a reductase known to reduce Cu^{2+} to its more toxic form, Cu^{1+}, and to be a direct target of elesclomol (*5*)] and six genes that encode either components of the lipoic acid pathway [lipolytransferase 1 (LIPT1), lipoyl synthase (LIAS), and dihydrolipoamide dehydrogenase (DLD)] or protein targets of lipoylation [the pyruvate dehydrogenase (PDH) complex, including dihydrolipoamide *S*-acetyltransferase (DLAT), pyruvate dehydrogenase E1 subunit alpha 1 (PDHA1), and pyruvate dehydrogenase E1 subunit beta (PDHB)] (*26*) (Fig. 3D). These observations were validated by an independent knockout screen that focused on 3000 metabolic enzymes (*27*) (Fig. 3E; fig. S4, A and B; and table S2). In addition, the metabolic enzyme screen showed that genetic suppression of complex I also rescued cells from copper-induced death (Fig. 3E; fig. S4, A and B; and table S2), consistent with our finding that chemical inhibitors of the ETC block cell death mediated by copper ionophores (Fig. 2).

Individual gene knockout studies further confirmed that deletion of *FDX1* and *LIAS* conferred resistance to copper-induced cell death (Fig. 3, F and G, and fig. S4, C to K), further strengthening a functional link between FDX1, the protein lipoylation machinery, and copper toxicity. Moreover, FDX1 deletion resulted in consistent resistance to a number of

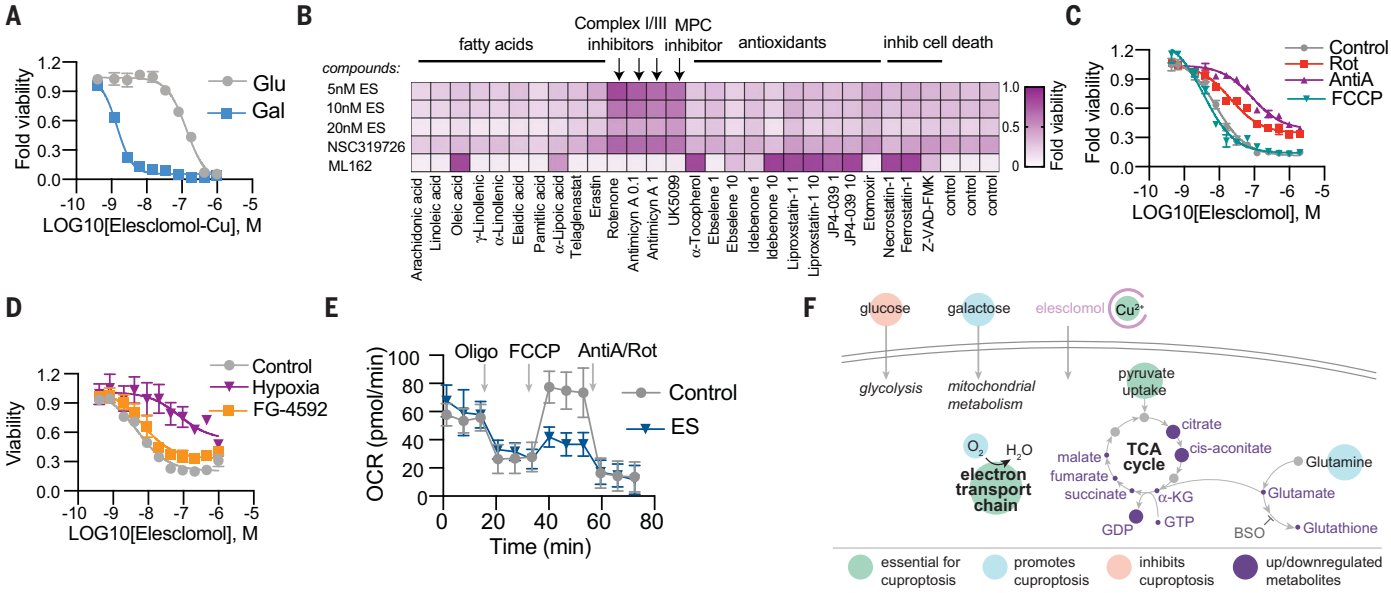

Fig. 2. Mitochondria respiration regulates copper ionophore–induced cell death. (**A**) Viability of NCIH2030 cells grown in media containing either glucose or galactose treated with elesclomol-Cu (ratio 1:1). (**B**) Viability of ABC1 cells pretreated with the indicated compounds (*x* axis) and then treated with elesclomol, NSC319726, or ML162 (*y* axis). The average of at least three replicates is plotted and color coded. MPC, mitochondrial pyruvate carrier. (**C**) Viability of ABC1 cells pretreated with 0.1 μM rotenone (Rot), 0.1 μM antimycin A (AntiA), or 1 μM FCCP and then treated with elesclomol. (**D**) Viability of ABC1 cells grown in control (21% O_2), hypoxia (1% O_2), or 50 μM FG-4592 (21% O_2) after treatment with elesclomol. (**E**) The oxygen consumption rate (OCR) was detected after treatment with 2.5 nM elesclomol (with 1 μM $CuCl_2$ in media) for 16 hours of ABC1 cells before (basal) and after the addition of oligomycin (ATP-linked), the uncoupler FCCP (maximal), or the electron transport inhibitor antimycin A/rotenone (baseline) (mean ± SD, $n = 8$). (**F**) Schematic of metabolites altered after elesclomol treatment of ABC1 cells. (Purple circles mark metabolites that change in abundance, as detailed in table S1. Larger circles are metabolites that are up-regulated, and smaller circles are metabolites that are down-regulated). GDP, guanosine diphosphate; GTP, guanosine triphosphate. For (A), (C), and (D), data are means ± SD, with $n \geq 3$.

copper ionophores (disulfiram, NSC319726, thiram, 8-HQ, and Zn-pyrithione) (fig. S5, A to G) but showed no substantial effects on either caspase activation (fig. S5, H to K), the potency of apoptosis-inducers (bortezomib, paclitaxel, and topotecan), or the ferroptosis-inducer ML162 (fig. S5, L to O). Of note, the strong connection between copper-mediated cell death and both FDX1 expression and protein lipoylation was lost at high concentrations of elesclomol (>40 nM) (fig. S4, L to P), thereby suggesting that off-target mechanisms of cell death may occur at such concentrations and possibly explaining conflicting mechanisms of action reported in the literature (*5*, *7*, *14*–*16*, *19*, *28*, *29*). Moreover, whereas the most copper-selective compounds (e.g., elesclomol, disulfiram, and NSC319726) lost killing activity when cells were grown under glycolytic conditions, compounds with more promiscuous metal-binding compounds (e.g., pyrithione and 8-HQ) killed independent of metabolic state. This result is consistent with copper's distinctive connection to mitochondrial metabolism-mediated protein lipoylation. (Fig. 2A and figs. S3, A to F, and S5, A to G).

FDX1 is an upstream regulator of protein lipoylation

Protein lipoylation is a highly conserved lysine posttranslational modification that is known to occur on only four enzymes, all of which involve metabolic complexes that regulate carbon entry points to the TCA cycle (*26*, *30*). These include dihydrolipoamide branched chain transacylase E2 (DBT), glycine cleavage system protein H (GCSH), dihydrolipoamide *S*-succinyltransferase (DLST), and DLAT, an essential component of the PDH complex. Lipoylation of these proteins is known to be required for enzymatic function (*30*) (Fig. 3D). Our findings that knockout of either FDX1 or lipoylation-related enzymes rescues cells from copper toxicity led us to explore whether FDX1 might be an upstream regulator of protein lipoylation. To test this hypothesis, we performed three analyses. First, we looked for evidence of coordinated dependencies across the Cancer Dependency Map (www.depmap.org), a resource of genome-wide CRISPR-Cas9 knockout screens in hundreds of cancer cell lines. Genes showing similar patterns of viability effects, even if subtle, suggest that they have shared function or regulation. Notably, FDX1 and components of the lipoic acid pathway were highly correlated in their viability effects across the cell line panel ($p < 0.0001$; Fig. 4A).

Second, we performed immunohistochemical staining for FDX1 and lipoic acid in 208 human tumor specimens and semiquantitative light-microscopic scoring by two independent pathologists. Expression of FDX1 and lipoylated proteins was highly correlated ($p < 0.0001$; Fig. 4, B and C, and fig. S6, A to D). Third, we determined whether FDX1 knockout affected protein lipoylation using a lipoic acid–specific antibody as a measure of DLAT and DLST lipoylation. FDX1 knockout resulted in complete loss of protein lipoylation, as measured by either immunoblot or immunohistochemistry (Fig. 4D and fig. S6, E to I), and also led to a significant drop in cellular respiration similar to the levels observed with the deletion of LIAS itself (Fig. 4E and fig. S6J). Furthermore, metabolite profiling after deletion of FDX1 led to an accumulation of pyruvate and α-ketoglutarate and depletion of succinate, as would be expected when protein lipoylation is compromised because of inhibition of the TCA cycle at PDH and α-ketoglutarate dehydrogenase (*31*) (Fig. 4F and table S3). Also of interest, we observed an increase in *S*-adenosylmethionine (SAM), a key substrate of LIAS in the lipoic acid pathway, consistent with FDX1 being a previously unrecognized upstream regulator of protein lipoylation.

Copper directly binds and induces the oligomerization of lipoylated DLAT

The experiments described above establish a connection between copper toxicity and protein lipoylation but do not establish a direct mechanistic link. We hypothesized that copper might directly bind to lipoylated proteins,

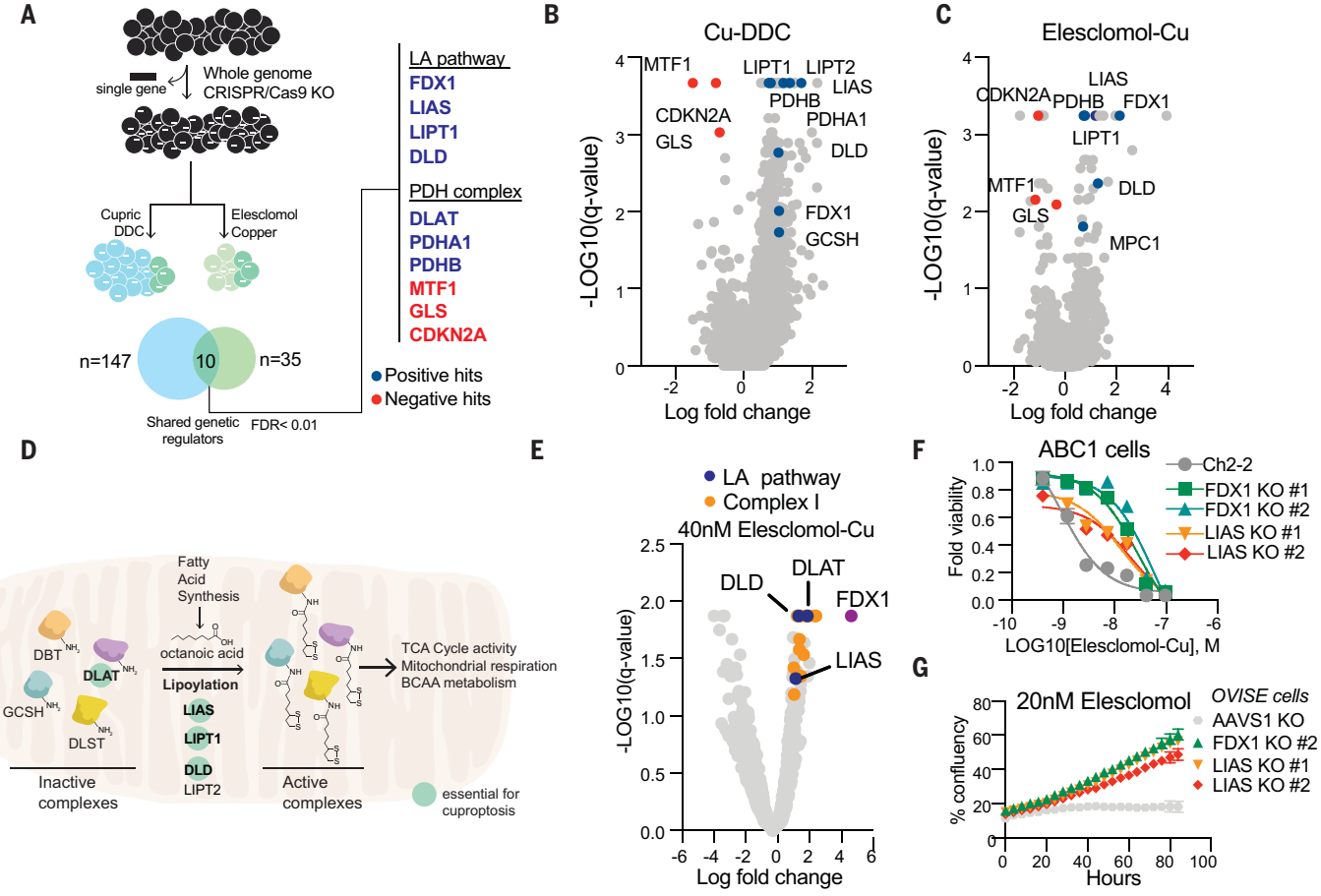

Fig. 3. FDX1 and lipoic acid genes are critical mediators of copper ionophore–induced cell death. (**A**) Whole-genome CRISPR-Cas9 positive selection screen using two copper ionophores (Cu-DDC and elesclomol-copper) in OVISE cells (schematic on the left). Overlapping hits with a false discovery rate (FDR) score <0.01 were analyzed (right). Positive hits (resistance) are marked in blue, and negative hits (sensitizers) are marked in red. (**B** and **C**) Summary scatter of the results of the screen in (A) for Cu-DDC (B) or elesclomol-Cu (C). (**D**) Schematic of the lipoic acid pathway. Genes that scored in our genetic screens are marked as essential for copper-induced cell death. BCAA, branched-chain amino acid. (**E**) Summary scatter plot indicating top hits in the metabolism gene–focused CRISPR-Cas9 gene knockout screen of A549 cells treated with 40 nM of elesclomol-Cu(II) (1:1 ratio). Genes associated with the lipoic acid pathway are marked in blue, complex I–related genes in orange, and FDX1 in purple. (**F**) Viability of ABC1 cells with CRIPSR-Cas9 deletion of *LIAS* or *FDX1* after treatment with elesclomol in the presence of 1 μM $CuCl_2$ in the media. (**G**) Growth curve measurements of OVISE cells with CRIPSR-Cas9 deletion of *LIAS* and *FDX1* in the presence of 20 nM elesclomol. For (F) and (G), data are means ± SD, with $n \geq 3$.

a possibility suggested by the observation that copper binds free lipoic acid with a measured dissociation constant of 10^{-17} (*32*). To test this hypothesis, we purified DLAT and DLST from cell lysates and found that these proteins bound to copper-charged resin but not to cobalt or nickel resins (Fig. 5A). When protein lipoylation was abrogated by FDX1 deletion (Fig. 4), DLAT and DLST no longer bound copper (Fig. 5B), suggesting that the lipoyl moiety is required for copper binding.

We noted that copper binding to lipoylated proteins did not simply lead to loss of function, given that deletion of the proteins rescues (not phenocopies) copper ionophore treatment. We proposed that copper binding to lipoylated TCA cycle proteins results in a toxic gain of function. Interestingly, we found that the copper binding to lipoylated TCA cycle proteins resulted in lipoylation-dependent oligomerization of DLAT that was detectable by nondenaturing gel electrophoresis (Fig. 5, B and C). Similarly, treatment of elesclomol-sensitive cells increased levels of DLAT oligomers and insoluble DLAT, whereas treatment of elesclomol-insensitive cell lines or FDX1 knockout (FDX1 KO) cells resulted in DLAT oligomerization only at much higher concentrations (Fig. 5, D and E, and fig. S7, A and B). Treatment with the strong reducing agent tris(2-carboxyethyl)phosphine (TCEP) and boiling eliminated the oligomeric form of DLAT (fig. S7, C to E), suggesting that the aggregates are disulfide-bond dependent. We confirmed these findings by immunofluorescence, observing pronounced induction of DLAT foci by short-pulse elesclomol treatment, whereas such foci were diminished in FDX1 KO, lipoylation-deficient cells (Fig. 5, F to H, and fig. S7F). These findings support a model where the toxic gain of function of lipoylated proteins after exposure to copper ionophores is mediated at least in part by their aberrant oligomerization. Mass spectrometric analysis also revealed that copper ionophore treatment leads to loss of Fe-S cluster proteins (Fig. 6, A and B) in an FDX1-dependent manner (Fig. 6C) as well as the induction of proteotoxic stress (Fig. 6, B and C; fig. S8A; and table S4). These findings are consistent with the observation in bacteria and yeast that copper can destabilize Fe-S–containing proteins (*33*–*35*). Whether such loss of Fe-S cluster proteins contributes to the copper ionophore death phenotype remains to be determined.

Copper-induced death mechanisms are shared by genetic models of copper homeostasis dysregulation

The experiments described to this point used copper ionophores to overcome the homeostatic mechanisms that normally keep intracellular

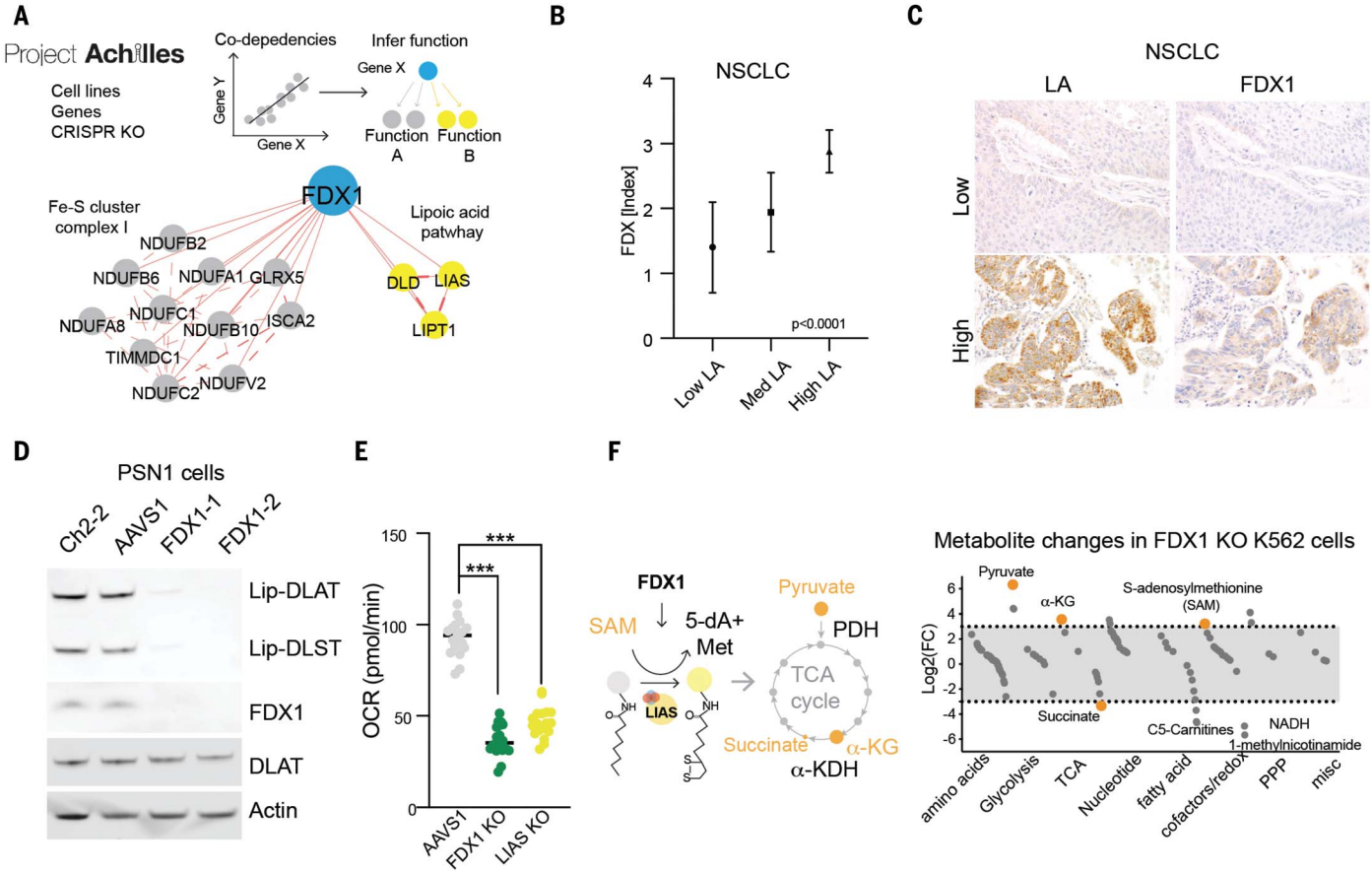

Fig. 4. FDX1 is an upstream regulator of protein lipoylation. (**A**) Correlation analysis of gene dependencies taken from the Achilles project. Presented is the gene network that correlates with *FDX1* deletion using FIREWORKS (*51*). The correlating genes are marked by their described functionality (lipoic acid pathway, and mitochondria complex I and Fe-S cluster regulation). (**B**) A tissue microarray of non–small cell lung carcinoma (NSCLC) (n = 57) was stained with lipoic acid (LA), and FDX immunohistochemistry (IHC) and expression was scored semiquantitatively by two pathologists (S.C. and S.S.), showing a strong direct correlation between LA and FDX expression (mean ± SD; $p < 0.0001$). (**C**) Representative cases of NSCLC with correlated low (top row) and high (bottom row) expression of LA and FDX1 by IHC. (**D**) Immunoblot of lipoylated proteins, FDX1, DLAT, and actin from extracts of PSN1 cells with deletion of *FDX1*. (**E**) Basal OCR as measured in PSN1 cells with CRIPSR-Cas9 deletion of *FDX1*, *LIAS*, or *AAVS1* genes (unpaired t test, ***$p <$ 0.001). (**F**) Plot of the average log2 fold change (FC) in metabolites between *FDX1* KO and *AAVS1* control K562 cell lines separated by functional annotations. Metabolites relevant to the lipoic acid pathway are marked in orange. α-KDH, α-ketoglutarate dehydrogenase; α-KG, α-ketoglutarate; NADH, reduced nicotinamide adenine dinucleotide; PPP, pentose phosphate pathway.

copper concentration low. These mechanisms include the copper importer SLC31A1 (CTR1) and the copper exporters ATP7A and ATP7B, which are encoded by genes that are mutated in the copper dysregulation syndromes Menke's disease and Wilson's disease, respectively (*3*, *36*) (Fig. 6D). To explore whether the mechanisms of copper toxicity associated with copper ionophore treatment are shared by these naturally occurring disorders of copper homeostasis, we examined three experimental models. First, we overexpressed SLC31A1 in human embryonic kidney (HEK) 293T and ABC1 cells, which dramatically increased sensitivity to physiological concentrations of copper (Fig. 6E and fig. S8B). Consistent with our findings using copper ionophores in wild-type cells, copper supplementation resulted in an overall reduction in proteins involved in mitochondrial respiration (fig. S8C and table S4), reduced protein lipoylation, reduced levels of Fe-S cluster proteins, and increased levels of HSP70 (Fig. 6F). Importantly, ferroptosis, necroptosis, and apoptosis inhibitors did not prevent copper-induced cell death in cells overexpressing SLC31A1 (Fig. 6G and fig. S8, D to F), whereas copper chelators, FDX1 KO, and LIAS KO each partially rescued cells from copper-induced cell death (Fig. 6, G and H, and fig. S8, D to G). In addition, depletion of the natural intracellular copper chaperone glutathione resulted in copper-dependent cell death (Fig. 6I), which was associated with reduced lipoylation and increased DLAT oligomerization (fig. S8, I and J) that was attenuated by FDX1 and LIAS KO, just as was observed with copper ionophore treatment of SCL31A1 wild-type cells (Fig. 6J and fig. S8H).

Lastly, we used a mouse model of Wilson's disease in which Atp7b deletion leads to intracellular copper accumulation and cell death with increasing animal age (*37*, *38*). Comparing the livers of aged Atp7b-deficient ($Atp7b^{-/-}$) mice with those of Atp7b heterozygous ($Atp7b^{-/+}$) and wild-type control mice, we observed loss of lipoylated and Fe-S cluster proteins, as well as an increase in Hsp70 abundance (Fig. 6K and table S5). These findings in mouse models of copper toxicity suggest that copper overload results in the same cellular effects as those induced by copper ionophores. Taken together, our data support a model whereby excess copper promotes the aggregation of lipoylated proteins and destabilization of Fe-S cluster proteins that results in proteotoxic stress and ultimately cell death (Fig. 6L).

Discussion

Copper is a double-edged sword: It is essential as a cofactor for enzymes across the animal kingdom, and yet even modest intracellular concentrations can be toxic, resulting in cell death (*2*). Genetic variation in copper homeostasis results in life-threatening disease (*39*, *40*), and both copper ionophores (*11*, *17*, *41*, *42*) and

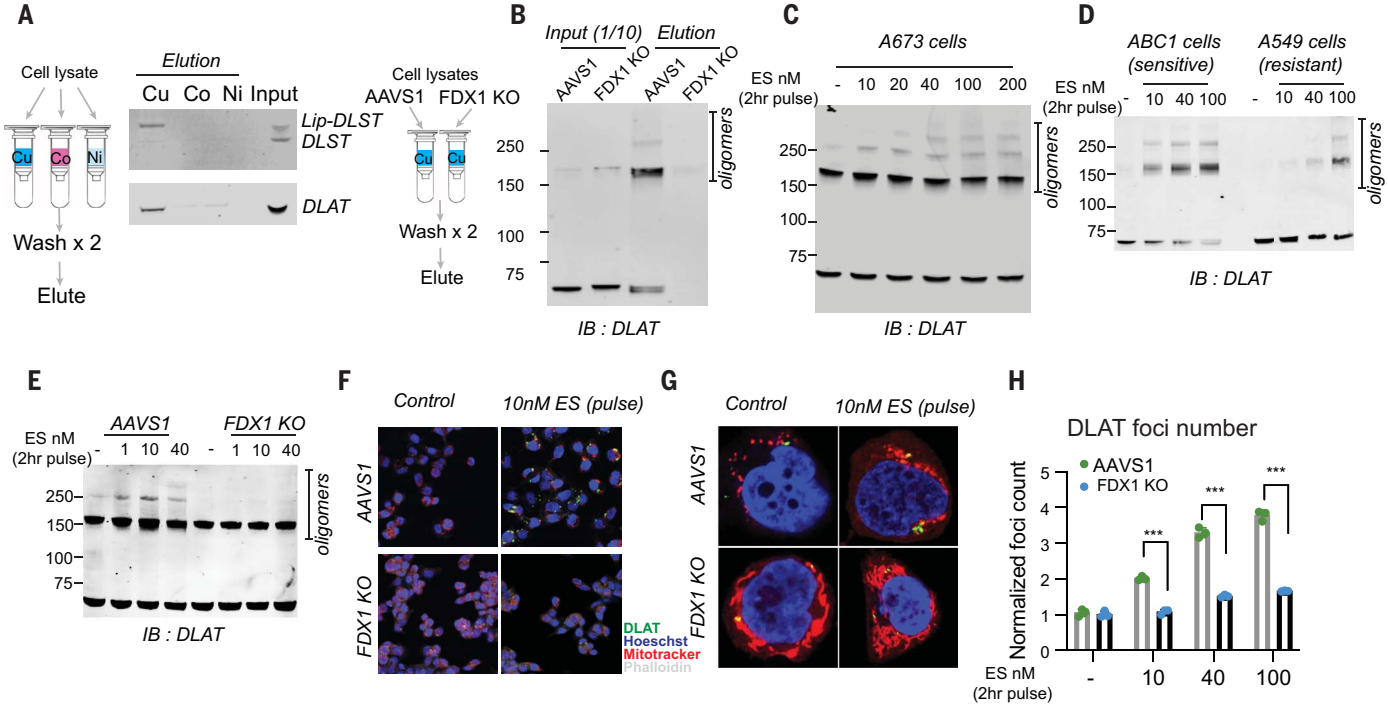

Fig. 5. Copper directly binds and promotes the oligomerization of lipoylated DLAT. (**A**) The binding of the indicated proteins to copper (Cu), cobalt (Co), and nickel (Ni) was assessed by immunoblot analysis of eluted proteins from the indicated metal-loaded resins. (**B**) Copper binding was assessed by loading cell lysates from either ABC1 AAVS1 or FDX1 KO cells on copper-loaded resin followed by washing and analysis of the eluted proteins. Input and eluted proteins are presented. IB, immunoblot. (**C**) Protein content was analyzed in A673 cells that were pulse-treated (2 hours) with the indicated concentrations of elesclomol. (**D**) Protein content was analyzed in ABC1 and A549 cells that were pulse-treated with the indicated concentrations of elesclomol. (**E** to **H**) AAVS1 control or FDX1 KO ABC1 cells were pulse-treated with the indicated concentrations of elesclomol for 2 hours; protein oligomerization was analyzed after 24 hours by immunoblotting (E) and both wide-field (F) and confocal (G) immunofluorescence imaging (green, DLAT–; red, Mitotracker; blue, Hoechst; white, phalloidin). (H) Foci were segmented and quantified in each condition [n = 3, and multiple unpaired t test analysis was conducted with the desired FDR(Q) = 1%; ***q < 0.001]. For (C) to (H), media were supplemented with 1 μM $CuCl_2$.

copper chelators (*43*–*46*) have been suggested as anticancer agents. However, the mechanism by which copper overload leads to cell death has been obscure. Here, we have shown that copper toxicity occurs by a mechanism distinct from all other known mechanisms of regulated cell death, including apoptosis, ferroptosis, pyroptosis, and necroptosis. We therefore propose that this previously uncharacterized cell death mechanism be termed cuproptosis.

We have shown that copper-induced cell death is mediated by an ancient mechanism: protein lipoylation. Notably few mammalian proteins are known to be lipoylated, and these are concentrated in the TCA cycle, where lipoylation is required for enzymatic function (*26*, *47*). Our study explains the relationship between mitochondrial metabolism and the sensitivity to copper-mediated cell death: Respiring, TCA-cycle active cells have increased levels of lipoylated TCA enzymes (in particular, the PDH complex), and the lipoyl moiety serves as a direct copper binder, resulting in lipoylated protein aggregation, loss of Fe-S cluster–containing proteins, and induction of HSP70, reflective of acute proteotoxic stress. The targets of copper-induced toxicity that we describe here in human cancer cells (lipoylation and Fe-S cluster proteins) are evolutionarily conserved from bacteria to humans, suggesting that copper-induced cell death might be also used by microorganisms where copper ionophores are naturally synthesized and exhibit antimicrobial activity (*48*, *49*).

In the case of genetic disorders of copper homeostasis (Wilson's disease and Menke's disease), copper chelation is an effective form of therapy (*50*). In cancer, however, the exploitation of copper toxicity has been less successful (*42*). Copper ionophores, including elesclomol, have been tested in clinical trials, but such testing occurred without the benefit of either a biomarker of the appropriate patient population or an understanding of the drug's mechanism of action. A phase 3 combination clinical trial of elesclomol in patients with melanoma showed a lack of efficacy in this unselected population, but a post hoc analysis of patients with low plasma lactate dehydrogenase (LDH) levels showed evidence of antitumor activity (*42*). Low LDH reflects a higher cellular dependency on mitochondrial metabolism (as opposed to glycolysis), consistent with our finding that cells undergoing mitochondrial respiration are particularly sensitive to copper ionophores and that this sensitivity is explained by their high levels of lipoylated TCA enzymes. Moreover, our observations that the abundance of FDX1 and lipoylated proteins is highly correlated across a diversity of human tumors and that cell lines with high levels of lipoylated proteins are sensitive to copper-induced cell death suggest that copper ionophore treatment should be directed toward tumors with such a metabolic profile. Future clinical trials of copper ionophores using a biomarker-driven approach should therefore be considered.

REFERENCES AND NOTES

1. B. E. Kim, T. Nevitt, D. J. Thiele, *Nat. Chem. Biol.* **4**, 176–185 (2008).
2. E. J. Ge *et al.*, *Nat. Rev. Cancer* **22**, 102–113 (2022).
3. S. Lutsenko, *Curr. Opin. Chem. Biol.* **14**, 211–217 (2010).
4. T. D. Rae, P. J. Schmidt, R. A. Pufahl, V. C. Culotta, T. V. O'Halloran, *Science* **284**, 805–808 (1999).
5. P. Tsvetkov *et al.*, *Nat. Chem. Biol.* **15**, 681–689 (2019).
6. B. B. Hasinoff, A. A. Yadav, D. Patel, X. Wu, *J. Inorg. Biochem.* **137**, 22–30 (2014).
7. S. Tardito *et al.*, *J. Am. Chem. Soc.* **133**, 6235–6242 (2011).
8. E. W. Hunsaker, K. J. Franz, *Inorg. Chem.* **58**, 13528–13545 (2019).
9. V. Oliveri, *Coord. Chem. Rev.* **422**, 213474 (2020).
10. S. M. Corsello *et al.*, *Nat. Cancer* **1**, 235–248 (2020).
11. D. Cen, D. Brayton, B. Shahandeh, F. L. Meyskens Jr., P. J. Farmer, *J. Med. Chem.* **47**, 6914–6920 (2004).
12. J. R. Kirshner *et al.*, *Mol. Cancer Ther.* **7**, 2319–2327 (2008).

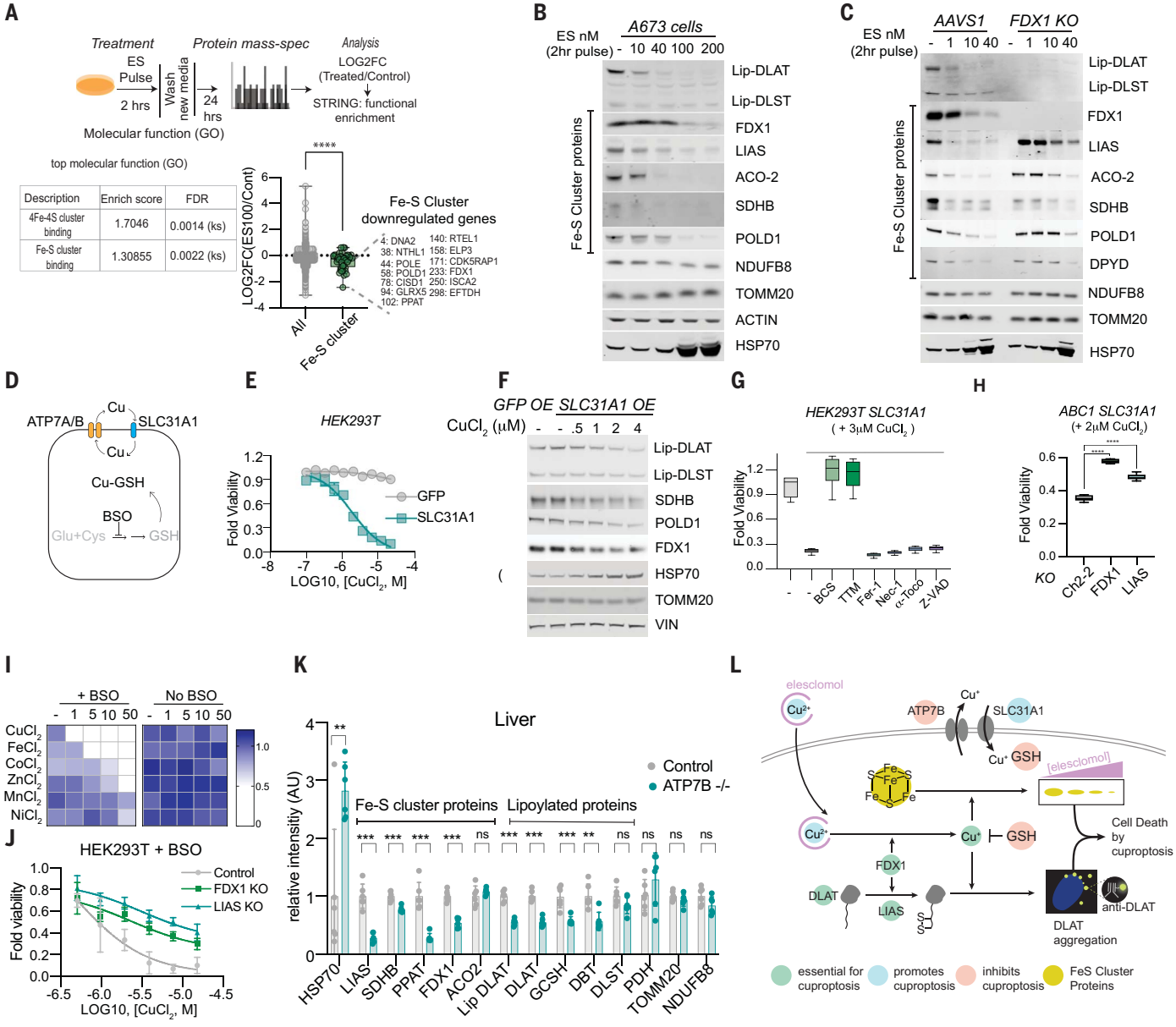

Fig. 6. Shared mechanisms in chemically and genetically induced copper-dependent cell death. (**A**) Proteomic analysis of control and elesclomol (100 nM) pulse-treated ABC1 cells 24 hours after treatment. Top [gene ontology (GO)] enriched categories are presented (table S4). (**B** and **C**) Protein content in A673 cells (B) and AAVS1 and FDX1 KO ABC1 cells (C) 16 hours after 2-hour pulse treatment with elesclomol. For (A) to (C), media were supplemented with 1 μM $CuCl_2$. (**D**) Copper homeostasis schematic. (**E** and **F**) HEK293T cells overexpressing green fluorescent protein (GFP) or SLC31A1 were analyzed for viability 72 hours after supplementation with $CuCl_2$ (E) and for protein content 24 hours after treatment (F). (**G**) Cells overexpressing SLC31A1 were pretreated with 10 μM necrostatin-1, 10 μM ferrostatin-1, 100 μM α-tocopherol, 40 μM Z-VAD-FMK, 10 μM TTM, or 40 μM bathocuproinedisulfonic acid (BCS). Viability was measured after 72 hours of cells growing in the presence or absence of 3 μM $CuCl_2$. (**H**) The viability of ABC1 Ch2-2, *FDX1*, and *LIAS* KO cells overexpressing SLC31A1 was analyzed 72 hours after treatment with 2 μM $CuCl_2$. In (G) and (H), viability is presented as box-and-whisker plots representing interquartile ranges (boxes), medians (horizontal lines), and range (whiskers). For both, $n \geq 5$, and an ordinary one-way analysis of variance (ANOVA) with multiple comparisons was conducted (****adjusted $p < 0.0001$). (**I**) Viability of control and 100 μM BSO–pretreated A549 cells 48 hours after treatment with the indicated metals. An average of three replicates is plotted. The color scale represents the relative viability. (**J**) Viability of control, *FDX1* KO, and *LIAS* KO HEK293T cells pretreated with 20 μM BSO and then with $CuCl_2$. (**K**) Protein content in $Atpb7b^{-/-}$ mouse livers (≥5 $Atpb7b^{-/-}$ mice) compared with control (six $Atpb7b^{+/-}$ mice and one wild-type mouse). Multiple unpaired *t* test analysis was conducted; ***$q < 0.001$, **$q < 0.01$, and ns is not significant. AU, arbitrary units. (**L**) Schematic of mechanisms that promote copper-induced cell death. For (E) and (J), data are means ± SD, with $n \geq 4$.

13. S. Tardito *et al.*, *J. Med. Chem.* **55**, 10448–10459 (2012).
14. M. Nagai *et al.*, *Free Radic. Biol. Med.* **52**, 2142–2150 (2012).
15. K. Shimada *et al.*, *Cell Chem. Biol.* **25**, 585–594.e7 (2018).
16. N. C. Yip *et al.*, *Br. J. Cancer* **104**, 1564–1574 (2011).
17. D. Chen, Q. C. Cui, H. Yang, Q. P. Dou, *Cancer Res.* **66**, 10425–10433 (2006).
18. N. Liu, H. Huang, Q. P. Dou, J. Liu, *Oncoscience* **2**, 457–466 (2015).
19. Z. Skrott *et al.*, *Nature* **552**, 194–199 (2017).
20. D. Tang, R. Kang, T. V. Berghe, P. Vandenabeele, G. Kroemer, *Cell Res.* **29**, 347–364 (2019).
21. B. A. Carneiro, W. S. El-Deiry, *Nat. Rev. Clin. Oncol.* **17**, 395–417 (2020).
22. R. Weinlich, A. Oberst, H. M. Beere, D. R. Green, *Nat. Rev. Mol. Cell Biol.* **18**, 127–136 (2017).
23. T. Bergsbaken, S. L. Fink, B. T. Cookson, *Nat. Rev. Microbiol.* **7**, 99–109 (2009).
24. S. J. Dixon *et al.*, *Cell* **149**, 1060–1072 (2012).
25. S. Elmore, *Toxicol. Pathol.* **35**, 495–516 (2007).

26. A. Solmonson, R. J. DeBerardinis, *J. Biol. Chem.* **293**, 7522–7530 (2018).
27. K. Birsoy *et al.*, *Cell* **162**, 540–551 (2015).
28. N. L. Reeder *et al.*, *Antimicrob. Agents Chemother.* **55**, 5753–5760 (2011).
29. A. A. Yadav, D. Patel, X. Wu, B. B. Hasinoff, *J. Inorg. Biochem.* **126**, 1–6 (2013).
30. E. A. Rowland, C. K. Snowden, I. M. Cristea, *Curr. Opin. Chem. Biol.* **42**, 76–85 (2018).
31. M. Ni *et al.*, *Cell Rep.* **27**, 1376–1386.e6 (2019).
32. J. Smirnova *et al.*, *Sci. Rep.* **8**, 1463 (2018).
33. D. Brancaccio *et al.*, *J. Am. Chem. Soc.* **139**, 719–730 (2017).
34. S. Chillappagari *et al.*, *J. Bacteriol.* **192**, 2512–2524 (2010).
35. L. Macomber, J. A. Imlay, *Proc. Natl. Acad. Sci. U.S.A.* **106**, 8344–8349 (2009).
36. T. Nevitt, H. Ohrvik, D. J. Thiele, *Biochim. Biophys. Acta* **1823**, 1580–1593 (2012).
37. S. Lutsenko, *Biochem. Soc. Trans.* **36**, 1233–1238 (2008).
38. A. Muchenditsi *et al.*, *Sci. Rep.* **11**, 5659 (2021).
39. O. Bandmann, K. H. Weiss, S. G. Kaler, *Lancet Neurol.* **14**, 103–113 (2015).
40. E. Gaggelli, H. Kozlowski, D. Valensin, G. Valensin, *Chem. Rev.* **106**, 1995–2044 (2006).
41. S. O'Day *et al.*, *J. Clin. Oncol.* **27**, 5452–5458 (2009).
42. S. J. O'Day *et al.*, *J. Clin. Oncol.* **31**, 1211–1218 (2013).
43. L. Cui *et al.*, *Nat. Biotechnol.* **39**, 357–367 (2021).
44. T. Tsang *et al.*, *Nat. Cell Biol.* **22**, 412–424 (2020).
45. C. I. Davis *et al.*, *Metallomics* **12**, 1995–2008 (2020).
46. D. C. Brady, M. S. Crowe, D. N. Greenberg, C. M. Counter, *Cancer Res.* **77**, 6240–6252 (2017).
47. J. A. Mayr, R. G. Feichtinger, F. Tort, A. Ribes, W. Sperl, *J. Inherit. Metab. Dis.* **37**, 553–563 (2014).
48. J. B. Patteson *et al.*, *Science* **374**, 1005–1009 (2021).
49. N. Raffa *et al.*, *Proc. Natl. Acad. Sci. U.S.A.* **118**, e2015224118 (2021).
50. A. Aggarwal, M. Bhatt, *Tremor Other Hyperkinet. Mov. (N. Y.)* **8**, 525 (2018).
51. D. R. Amici *et al.*, *Life Sci. Alliance* **4**, e202000882 (2020).

ACKNOWLEDGMENTS

We thank J. Markley, H. Adelmann, M. Slabicki, V. Wang, and H. Keys for constructive discussion and help with genetic screens. We thank T. Woo for help with immunohistochemistry and immunofluorescence studies and A. Muchenditsi for help with the Atp7b mice. We thank C. Lewis (Whitehead metabolomics), W. Salmon (Whitehead imaging), and R. Rodrigues (Harvard Medical School–Thermo Fisher Scientific Center for Multiplexed Proteomics proteomic facility) for technical help. We thank M. O'Reilly for help with the design of the figures. We thank the Image and Data Analysis Core at Harvard Medical School for coding support. **Funding:** This work was supported by National Cancer Institute (NCI) grant 1 R35 CA242457-01 (T.R.G.), Novo Holdings (T.R.G. and P.T.), NCI grant K08 CA230220 (S.M.C.), National Institute of General Medical Sciences grant T32-GM007748 (S.C.), research and recruitment funding by Boston Children's Hospital (B.P. and N.K.), NCI grant R01-CA194005, NCI grant U54-CA225088, and the Ludwig Center at Harvard (S.S.). **Author contributions:** P.T. conceptualized the project, conducted experiments, collected data, and analyzed results. M.A. and M.D. assisted with experiments. L.J.-C., J.R., and M.K. assisted with data analysis. R.H. and R.D.S. performed the whole-genome CRISPR-Cas9 screens under supervision from S.M.C. S.C. and S.S. performed the tissue microarray staining scoring and visualization, and A.V. assisted with the microscopy analysis. B.P. and N.K. performed and analyzed the metabolomics experiments. S.L. provided study material and experimental advice. J.K.E. and E.F. provided reagents and experimental advice. T.R.G. supervised the research. P.T. and T.R.G. wrote the manuscript. **Competing interests:** S.M.C. and T.R.G. receive research funding unrelated to this project from Bayer HealthCare and Calico Life Sciences. T.R.G. receives research funding related to this project from Novo Holdings, recently held equity in FORMA Therapeutics, is a consultant to GlaxoSmithKline and Anji Pharmaceuticals, and is a founder of Sherlock Biosciences. S.S. is a consultant for RareCyte, Inc. P.T. and T.R.G. are inventors on the patent application PCT/US21/19871 submitted by the Broad Institute entitled "Method of treating cancer." J.E. is currently an employee of Kojin Therapeutics. The other authors declare no competing interests. **Data and materials availability:** All data are available in the manuscript or the supplementary materials.

SUPPLEMENTARY MATERIALS

science.org/doi/10.1126/science.abf0529
Materials and Methods
Figs. S1 to S8
Tables S1 to S5
References (*52*–*63*)
MDAR Reproducibility Checklist

View/request a protocol for this paper from *Bio-protocol*.

30 September 2020; resubmitted 18 January 2022
Accepted 4 February 2022
10.1126/science.abf0529